Eight-Wavelength, Dual Detection Channel Instrument for Near-Infrared Time-Resolved Diffuse Optical Spectroscopy

Marco Renna, Mauro Buttafava, Anurag Behera, Marta Zanoletti, Laura Di Sieno, Alberto Dalla Mora, Davide Contini, and Alberto Tosi, *Member, IEEE*

***Abstract*—In this paper, we present an innovative instrument for near-infrared time-resolved spectroscopy. The system is based on eight custom-designed pulsed diode lasers emitting at different wavelengths in the near-infrared region (635–1050 nm), all exhibiting an average optical power higher than 1 mW at 40 MHz pulse repetition rate, two custom-made single-photon detectors based on wide-area silicon photomultipliers and two time-measurement units based on a custom time-to-digital converter with 10 ps timing resolution. The system instrument response function has a width narrower than 160 ps (fullwidth at half-maximum) and stability better than $\pm 1\%$ for several hours for all the wavelengths. All the components of the instrument were designed in order to be compact. The entire system will be hosted in a standard 19 inches, 5U rack case (size $48 \times 38 \times 20$ cm^3). The system communicates with the external computer through a USB 2.0 link and is designed to be employed in a clinical environment. The proposed instrument, thanks to the reduction of its cost and dimensions, paves the way to a wider diffusion of multiwavelengths near-infrared time-resolved spectroscopy systems.**

***Index Terms*—Diffuse optics, near-infrared spectroscopy, pulsed laser, single-photon detector, time-resolved, time-correlated single-photon counting, time-to-digital converter.**

I. Introduction

OVER the last few years, the interest towards photonic instruments have seen an exponential growth in several fields, from automotive to industrial automation, chemistry, biomedicine and many others. Among them, the use of photonic instrumentation to noninvasively probe human biological tissues, agricultural or pharmaceutical products through the use of monochromatic light sources emitting in the near-infrared region [1]–[4] is generally called Near-InfraRed Spectroscopy (NIRS). In detail, the theory of photon migration in diffusive media, generally known as Diffuse Optics (DO) [5], demonstrated how it is possible to retrieve information on the sample constituents [6]–[8]. The easiest implementation of DO techniques is based on a Continuous Wave (CW) light and detection, and the low system complexity guarantees low cost and small dimensions, leading to a wide diffusion in both the clinical and the commercial fields, where compact systems are currently under development to be equipped in wearable devices [9]. Nevertheless, this approach has several drawbacks [10], as the impossibility, using a single source-detector pair, to distinguish between photon scattering and absorption phenomena within the sample and a limited depth sensitivity and selectivity [11], [12]. A time-resolved approach (also referred to as Time-Domain – TD approach) allows to distinguish between scattering and absorption effects and breaks the trade-off between penetration depth and source-detector distance, making them almost independent [12]–[14]. Indeed, the capability to recover the photon Distribution of Time-Of-Flight (DTOF) curves adds a further dimension to the measurement, as contributions coming from shallow and inner layers of the sample can be correctly distinguished [15]. Additionally, TD approaches allow reducing the source-detector distance with respect to CW systems, leading to higher SNR and better lateral resolution [16], which reaches the physical limit when the injection and collection points coincide [17], [18].

Recent achievements in the development of compact laser sources, single-photon detectors and time-measurement electronics [19]–[21], allowed to develop many instrument exploiting DO: from complex and extremely expensive systems with outstanding performance for laboratory use, down to more compact solutions for clinical environments and even portable devices [19], [22]. The main drawbacks of TD instruments with respect to CW ones are the higher costs and system complexity due to the use of high-performance pulsed laser sources, single-photon detectors and timing electronics with picosecond resolution [9]. In fact, most of the existing portable instruments for TD-NIRS are custom-made prototypes based on off-the-shelf photonic components (either general purpose pulsed laser diodes or white-light fiber lasers, photomultipliers, time-correlated single-photon counting modules), thus exhibiting strong limitations in terms of cost, dimensions, robustness and complexity.

Manuscript received April 6, 2018; revised July 16, 2018; accepted July 23, 2018. Date of publication August 8, 2018; date of current version August 21, 2018. This work was supported in part by the European Union's Horizon 2020 research and innovation programme under Grant agreement 688303, and in part by the European Commission under H2020 framework with the BITMAP project 675332. *(Corresponding author: Marco Renna.)*

M. Renna, M. Buttafava, and A. Tosi are with the Dipartimento di Elettronica Informazione e Bioingegneria, Politecnico di Milano, Milano 20133, Italy (e-mail: marco.renna@polimi.it; mauro.buttafava@polimi.it; alberto.tosi@polimi.it).

A. Behera, M. Zanoletti, L.-D. Sieno, A.-D. Mora, and D. Contini are with the Dipartimento di Fisica, Politecnico di Milano, Milano 20133, Italy (e-mail: anurag.behera@polimi.it; marta.zanoletti@polimi.it; laura.disieno@polimi.it; alberto.dallamora@polimi.it; davide.contini@polimi.it).

Color versions of one or more of the figures in this paper are available online at http://ieeexplore.ieee.org.

Digital Object Identifier 10.1109/JSTQE.2018.2863570

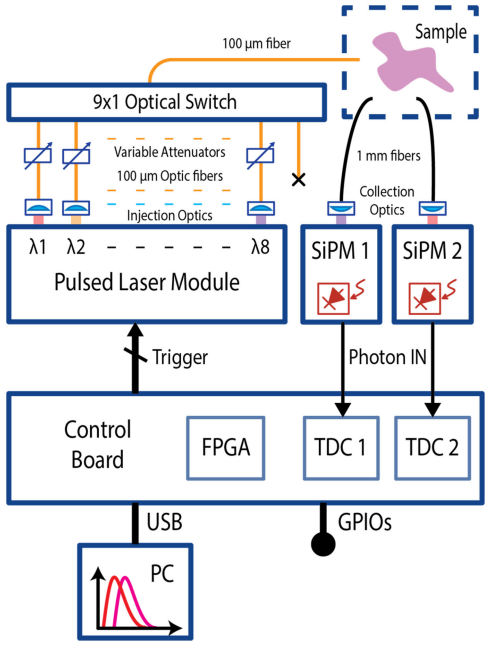

Fig. 1. Simplified block diagram of the instrument. The FPGA on the control board provides the trigger signals for the laser sources starting from a high-stability reference clock source. The emitted optical pulses are coupled to eight 100 μm-core optical fibers, attenuated and fed to a 9 $\times$ 1 optical switch, used to select the output wavelength. The optical pulses provided at the output of the switch are injected into the sample through a 100 μm-core fiber. Backscattered light is collected by two 1 mm-core optical fibers and coupled to the two SiPM-based detectors. The voltage pulses corresponding to the detection of a photon (see 'Photon IN' signals) are connected to two independent TDCs for measuring their arrival time. The FPGA acquires the TDC results and builds up the histograms of the photon arrival times for each detection channel and transfer the final curves to the external computer through a USB 2.0 link.

This work aims at developing an innovative eight wavelengths, two detection channels instrument for TD NIRS suitable for a clinical environment, by developing custom-made state-of-the-art photonic components for guaranteeing optimal performance at reduced costs, thus fostering the diffusion of time-resolved spectroscopy instruments in the biomedical field. The instrument we developed has narrow Instrument Response Function (IRF) thus allowing to challenge the system even in critical situations (e.g., high absorbing medium or layered structures) where the shape of the IRF is a crucial parameter to obtain robust and accurate measurements. Two detection channels also allow the implementation of a double-distance measurement scheme (one light injection point and two detection points placed at two different distances), improving accuracy in estimating constituents in layered tissues. Furthermore, a wide range of wavelengths permits better discrimination between various constituents like lipids, collagen and water, in addition to oxygenated and de-oxygenated hemoglobin, providing more information on the sample.

II. System Design

In this section we describe in detail the complete instrument. Fig. 1 shows its simplified block diagram with:

1) Eight custom-made pulsed laser sources based on commercially available edge-emitting laser diodes at eight different wavelengths in the near-infrared region, operating in gain-switching mode.
2) Two custom-made single-photon detectors based on commercially available wide-area Silicon PhotoMultipliers (SiPMs) operating in photon-counting mode.
3) Two time-measurement units based on custom-made Time-to-Digital Converter (TDC) integrated circuit fabricated in 0.35 μm HV-CMOS technology [23].
4) A custom FPGA-based control board hosting the time-measurement units, managing the instrument measurement procedures and providing communication with the external computer through a USB 2.0 link.

Optical pulses generated by the eight laser sources are coupled into 100 μm-core optical fibers, and each one is fed to an independent in-fiber, user-adjustable, variable attenuator to regulate the output optical power of the eight laser sources, allowing to equalize the intensity of optical signals collected from the sample, still guaranteeing laser safety when performing in-vivo measurements. Each optical attenuator is specifically tuned at the respective laser center wavelength, providing up to 40 dB attenuation, and is controlled by the control board through a dedicated I^2C bus. The optical attenuator outputs are connected to a 9 $\times$ 1 optical switch, allowing to select the output wavelength with only 10 ms dead-time and negligible losses. The ninth channel input is kept unconnected and it is selected when no laser signal has to be provided (i.e., no measurement is running), in compliance with safety regulation.

The output optical pulses are delivered to the sample through a 100 μm-core optical fiber and photons re-emitted from the sample are collected by two 1 mm plastic optical fibers, each one connected to a SiPM-based single-photon detector, and detector outputs are directly fed (through 50 Ω coaxial cables) to the inputs of the time-measurement units.

The FPGA has various tasks: i) controls the instrument measurement routine; ii) provides the trigger signals to the laser pulser module; iii) controls the variable optical attenuators and the 9 $\times$ 1 optical switch; iv) reconstructs the histogram of the photon arrival times per each detection channel; v) provides the results to an external PC.

Measurement parameters are set by the user via a graphical user interface and guarantee high system reconfigurability, which makes the instrument suitable for a various range of applications other than time-resolved spectroscopy, such as time-resolved photoluminescence/fluorescence spectroscopy, fluorescence correlation spectroscopy and others.

Since the optical switch can output only one wavelength at a time, going through all the eight wavelength prevents the possibility to use the instrument to follow dynamic processes with more than 2 or 3 wavelengths. Indeed, the instrument in its full eight-wavelengths configuration was designed to perform quasi-static measurements, which are compatible with a measurement time of a few tens of seconds.

The instrument will be housed in a standard 19-inches rack case (dimensions are 48 $\times$ 38 $\times$ 20 cm^3) and communicates with a PC via a USB 2.0 link. Thanks to eight General Purpose Input/Output (GPIO) lines (directly linked to the control board for configurable functions) and five wide-bandwidth

connections, this module can be easily integrated in complex systems for multi-modal measurements. Power supply is from either 230 V AC (50 Hz) or 110 V AC (60 Hz) power lines, which are converted by an internal medical-grade AC/DC power supply to a 24 V DC and then a dedicated power board distributes the various power supplies to the sub-components. The overall power consumption is less than 60 W.

The following sections describe in detail the main instrument components.

A. Pulsed Laser Module

A pulsed laser source suitable for a near-infrared time-resolved spectroscopy instrument should provide powerful optical pulses with a temporal width as narrow as possible, generally lower than 250 ps FullWidth at Half-Maximum (FWHM). Furthermore, high stability for both power and shape of the optical pulse over time and temperature are required, thus enabling long-time monitoring applications. Light sources based on supercontinuum laser generation have been widely used in laboratory setups for NIRS measurements [24], providing narrow optical pulses (in the order of a few picoseconds) with high average power (a few Watts on broadband wavelength range) at repetition rates of tens of MHz [25]. Despite the outstanding optical performance, supercontinuum laser sources are expensive, bulky and complex systems.

Pulsed laser sources based on edge-emitting laser diodes are among the best solutions for TD NIRS instrument as they provide a good compromise between optical performance, dimensions, robustness, and ease-of-use. Many companies provide laser systems based on pulsed laser diodes featuring an average optical power of a few mW at a pulse repetition rate up to 80 MHz and a temporal width of the optical pulses in the order of 100–150 ps, with a variety of wavelengths (see [26], [27] and others). However, a complete set of eight different laser heads would lead to an overall cost of tens of thousands of euros. Furthermore, these laser systems are normally designed as general purpose pulsed laser and are not customizable in terms of size, functionalities, etc.

Given the need of a large set of wavelengths in the near-infrared region with state-of-the-art optical performance and reduced costs and dimensions, we decided to develop an eight-wavelength pulsed laser module based on commercially available edge-emitting laser diodes mounted in standard TO package and custom driving electronics. We chose TO package as a reference for our design since it is employed for laser diodes with a large number of available wavelengths and optical powers. Additionally, a wide range of optical components for laser diode housing and fiber coupling are available off-the-shelf from different vendors, like the collimation optics that we employed.

The complete pulsed laser sources module is shown in Fig. 2. Its core is the laser diode pulser board, an upgraded version of the laser diode driver described in [22]. Each channel has its own adjustable parameters for a tight regulation of optical performance of each laser diode. A pulse shaper circuit provides voltage pulses with a temporal duration adjustable between 0.5 and 5 ns, which are AC-coupled to the gate of a high-bandwidth pseudomorphic High Electron Mobility Transistor (pHEMT), used to deliver fast current pulses (rise/fall times faster than 100 ps and 1 A peak current) to the laser diode for driving it in gain-switching regime [28]. With respect to the previous design, we adopted LVDS signaling which allowed us to remove the front-end comparator, reducing cost and power dissipation of each pulser. We also revised the current driver circuit loop in order to reduce stray inductances and capacitances, and the current loop area, mitigating ElectroMagnetic Interference (EMI) effects. The performance obtained with the entire set of selected laser diodes are listed in Table I, with a pulse-width always lower than 135 ps FWHM and an average optical power ranging from 1 to 9 mW at 40 MHz repetition rate, depending on the wavelength. Optical performance are strictly dependent on the selected laser diode, in particular when driven in gain-switching regime. The improvements here introduced compared to the previous version (see [22]) can be assessed analyzing the laser sources at 670 and 830 nm (same laser diodes used). We obtained a pulse-width equal to 135 ps (FWHM) and a free-space average optical power equal to 8.7 mW for the 670 nm laser diode and 110 ps and 5.2 mW for the 830 nm one, when pulsed at 40 MHz repetition rate, thus doubling the average output optical power and halving the temporal duration of the optical pulse with respect to the previous design. Moreover, with the redesign the laser diode pulser can reach a higher maximum pulse-rate, user-adjustable between 100 kHz and 120 MHz at 10 kHz steps.

TABLE I
SUMMARY OF PERFORMANCE FOR THE PULSED LASER SOURCES

Wavelength [nm]	*Free-space average optical power*[a] *[mW]*	*Fiber-coupled average power*[a] *[mW]*	*Pulse-width*[b] *[ps]*
635	4.7	3.3	105
670	8.7	4.7	135
730	1.45	1.1	75
830	5.2	4.1	110
852	6.25	2.6	115
915	4.9	3.4	100
980	4.2	3.1	95
1050	7.2	3.5	115

[a]Measured at 40 MHz pulse repetition rate.
[b]Temporal duration of the optical pulse, FullWidth at Half-Maximum.

In order to guarantee optical stability better than $\pm 1\%$ over time and ambient temperature variations, two thermal systems are used: i) a heating circuit sets the working temperature of the laser diode drivers at 55 °C, preventing thermal drifts which may lead to a temporal shift of the laser pulse emission (heating was preferred to cooling in order to reduce power dissipation); ii) the laser diode is kept below room temperature (16 °C) by means of a ThermoElectric Cooler (TEC) and a custom mechanical assembly, which hosts the TO package mounted inside

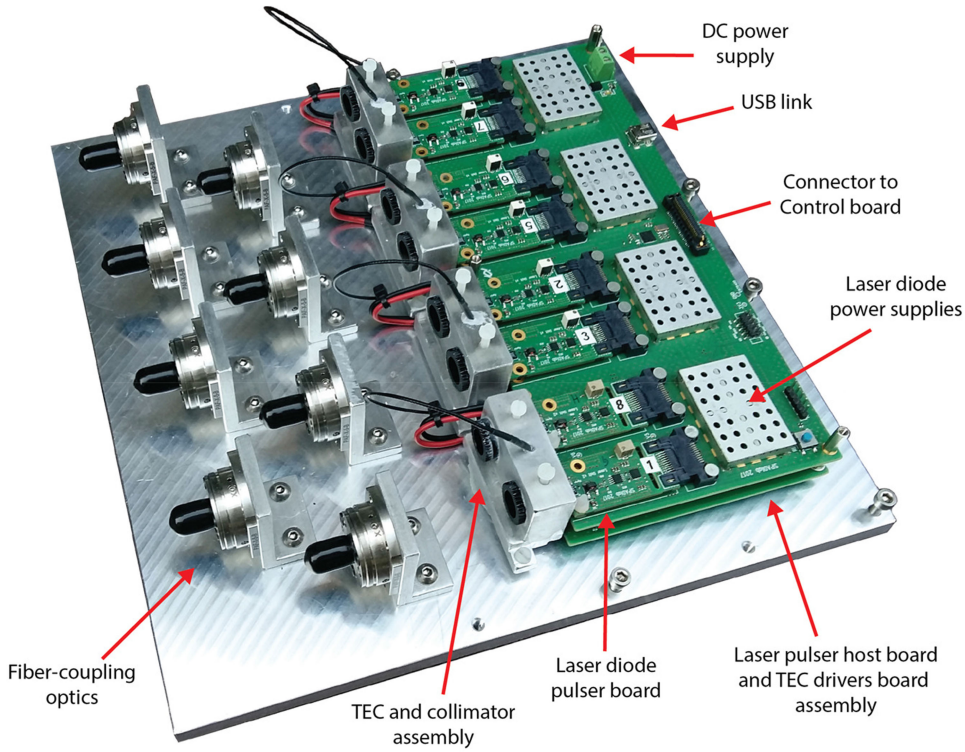

Fig. 2. Picture of the developed pulsed laser module. The eight laser heads are connected to a custom PCB (in picture referred as Laser pulser host board), which features 8 independently-adjustable power supplies, one for each laser source. The power supply circuitries are coupled two-by-two and enclosed in a metal shield in order to reduce ElectroMagnetic Interference (EMI) effects on sensible nodes, such as laser diode power supplies. A microcontroller in the laser pulsers host board guarantees correct turn-on/turn-off procedures, besides managing the communication with the control board. The board also features a USB 2.0 link for debug mode (not used in standard operating conditions). The measurement trigger signal is generated by the control board and fed to the laser diode pulsers through a 100 Ω differential twinaxial cable assembly and matched impedance routes on the laser diode pulsers host board.

standard collimation optics. Laser heads are coupled two-by-two in the mechanical assembly to reduce dimensions and number of components, as all the selected laser diodes can be operated at the same temperature. The output of each laser diode is coupled into a 100 μm-core optical fiber through a commercial optical system with five degrees of freedom and rotational adjustment. A coupling efficiency ranging from 40% to 80% (from laser diode output to the fiber output tip) has been achieved, with differences depending on the divergence of each laser diode.

The eight laser diode pulsers are mounted on a single PCB (in Fig. 2 referred as laser pulsers host board), which provides independent, user-adjustable power supplies to the laser diodes and is equipped with a microcontroller in order to guarantee a correct turn-on/off procedure, avoiding any damage due to incorrect biasing of the laser diodes. The microcontroller manages the communication with the pulsed laser module via I^2C peripherals (used to monitor the laser diode average current and temperature of both TEC assembly and laser driver circuitry) and communicates with the FPGA hosted on the instrument control board for receiving all the parameters needed to program the laser diode drivers.

Eight trigger signals are provided by the FPGA to the eight laser diode pulsers through matched impendence routes. Time-delay introduced by electrical signal routes is matched for all the eight laser sources, providing an almost synchronous emission for all the selected wavelengths (about 3 ns maximum delay between centroids of DTOF curves obtained at all the eight different wavelengths), thus simplifying the design of measurement readout electronics.

Finally, below the laser pulsers host board, a second PCB embeds all the circuitry required to accurately control the four independent TECs with thermal regulation of the laser diode temperature with 0.1 °C precision.

The overall pulsed laser module (including both electronic circuits and fiber-coupling optics) has a $26 \times 26 \times 8\text{cm}^3$ volume, maximum power consumption lower than 30 W and requires a single 24 V DC power supply. The compact assembly, the choice of commercially available laser diodes and components and the redesign of the signal chain leaded to a reduction of the costs for eight laser heads (including the control circuitry) of about five times with respect to commercially-available solutions with comparable performance. Finally, the high modularity of the pulsed laser module allows to tailor the output wavelengths to the specific application, by just changing the laser diode.

B. *SiPM-Based Single-Photon Detectors*

To limit the measurement timing jitter added to the DTOF curves, the detector Single-Photon Timing Resolution (SPTR) should be in the order of tens of picoseconds, while the

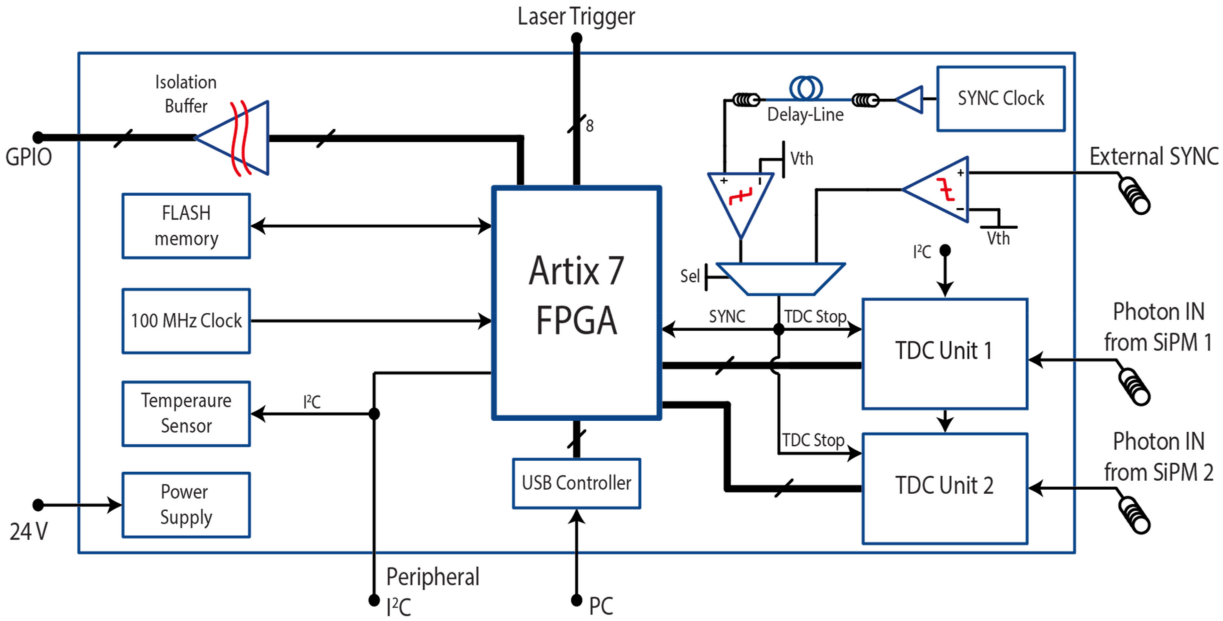

Fig. 3. Simplified block diagram of the instrument control board. The Artix 7 FPGA (Xilinx Inc.) acquires data from the two time-measurement units, reconstructing the TCSPC histograms that are provided to the external PC through an USB 2.0 controller. A high stability 100 MHz clock source sets the time-base of the FPGA, which manages the instrument measurement routine, actively selecting the measurement repetition frequency through a crystal-based programmable oscillator, providing the trigger signals to the pulsed laser module and communicating with its microcontroller. An isolation buffer is used to provide eight General Purpose Input/Outputs (GPIOs) for customizable signals, still guaranteeing electrical isolation to the FPGA, whose firmware is stored in a FLASH memory for a correct turn-on procedure of the instrument. An I^2C bus is used to control various peripheral systems throughout the instrument, such as the TEC drivers, the optical variable attenuators, temperature sensor, etc.

Photon Detection Efficiency (PDE) must be as high as possible in the near-infrared range in order to improve the signal-to-noise ratio. Vacuum-tube based photodetectors, such as PhotoMultiplier Tubes (PMT) or MicroChannel Plates (MCP), provide good PDE (in some cases more than 40% at 700 nm), and a sufficiently narrow SPTR [29]. Despite the good performance and the wide-active area offered by PMTs and MCPs, they present some limitations for the use in a clinical environment in terms of robustness (high level of illumination may damage photocathodes) and costs. Detector modules based on silicon Single-Photon Avalanche Diode (SPAD) overcome these issues and can fit the application, as they generally exhibit a SPTR lower than 30 ps (FWHM) and a PDE higher than 60% at 500 nm and still 12% at 800 nm [30], [31]. Unfortunately, wide collection area is mandatory in order to improve light harvesting [19]. Therefore, the use of SPADs in this design is demoted due to their small detection area (tens or hundreds μm diameter). SiPMs recently have seen a technological boost, demonstrating to be a feasible solution in single-photon applications where a large active-area is required, with small compromise on the detector Dark Count Rate (DCR) and SPTR [32], [33].

In the presented instrument, the two detection modules are based on an improved version of the custom-made single-photon detector described in [34] and exploited in [22] where, thanks to a new $1.3 \times 1.3\,mm^2$ silicon SiPM detector (commercially available from Hamamatsu Photonics KK) and a two-stage RF amplification circuit, state-of-the-art performance are obtained, with a SPTR equal to 70 ps (FWHM) and a PDE equal to 38% at 500 nm and 8% at 800 nm. Each SiPM is housed in a standard TO-8 package and cooled at 10 °C by a two-stage TEC to reduce the detector DCR to about 10 kcps for SiPM2 and 50 kcps for SiPM1 (difference due to SiPM fabrication process variability), while having an afterpulsing probability still lower than 1%. The two-stage amplifier is based on Monolithic Microwave Integrated Circuits (MMICs) and amplifies the avalanche signal from the SiPM, providing fast voltage pulses (sub-nanosecond rise/fall times) with an amplitude of few hundreds of mV, guaranteeing low timing jitter and good immunity to EMI effects. The detector is housed in a compact $50 \times 110 \times 40\,mm^3$ aluminum case and requires a single 15 V DC power supply, with a maximum power consumption of 8 W each (at the maximum count rate of 150 Mcps).

Photons re-emitted by the sample are collected through two 1 mm-core optic fiber and focused on the detector active area through a custom optical system.

C. System Control Board and Time-Measurement Electronics

The capability to measure photon arrival times with high accuracy and linearity is of utmost importance in order to correctly reconstruct the DTOF curves of photons re-emitted by the sample. Commercially-available TCSPC acquisition systems have excellent linearity performance (<1% of Least Significant Bit, LSB) with picosecond timing resolution and a single-shot precision lower than 10 ps [35], [36]. These systems are too bulky and expensive for being embedded in a compact instrument for TD NIRS measurements. In this work we designed a custom-made time-measurement unit and we integrated two of them on

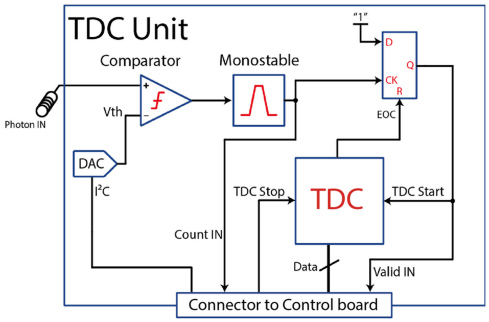

Fig. 4. Simplified block diagram of the time-measurement unit. The two time-measurement units are connected to the instrument control board for the readout of the measured time intervals. The *TDC Stop* signal arrives from the control board. The *Count IN* and *Valid IN* are provided to the FPGA in order to monitor the detector count rate and the TDC conversion rate.

the instrument control board (see Fig. 3). The latter is based on a high-performance FPGA (Xilinx Artix 7), which runs the measurement routine and builds the TCSPC histograms for the two detection channels starting from the photon arrival times provided by the two TDCs.

Starting from a high-quality crystal-based programmable oscillator the FPGA provides the eight independent LVDS trigger signals for the pulsed laser module, with a measurement repetition rate variable between 1 and 100 MHz (typically set to 40 MHz). A delay line made through a coaxial cable is used to correctly match the delays for the pulsed laser sources and the time-measurement instruments, avoiding digital delay-lines within the FPGA. The "External SYNC" input, which is fed to a wide-bandwidth (8 GHz) comparator (with user-adjustable threshold variable between -3 V and 3 V), can be used as an external trigger. A conditioning logic circuit selects the reference source (between the internal and the external one) to be used for running the TCSPC measurement routine, thus increasing system flexibility and allowing to integrate this instrument in various measurement setups.

The time-measurement unit (whose block diagram is shown in Fig. 4) is based on a custom TDC ASIC [23], with a Full-Scale Range (FSR) of 160 ns, a timing resolution of 10 ps, a single-shot precision of 40 ps (FWHM) and a Differential Non-Linearity (DNL) equal to 0.9% of LSB (RMS). When a photon is detected, a voltage pulse (whose rising-edge marks its arrival) is discriminated by a wide-bandwidth comparator with user-adjustable threshold. The signal is then provided to a pulse-shaper circuit and a D-Flip Flop is used for signal conditioning, as described in [37], thus giving the *TDC Start* signal to the TDC ASIC only when another start-stop conversion is not already running. Since this approach improved the overall DNL and timing jitter of the instrument, as it avoids conditioning logic circuitry within the FPGA that would lead to stronger crosstalk, we adopted the same circuital solution (based on discrete components on the control board) to generate also the *TDC Stop* signal. This resulted in an improvement of the performance of the time-measurement units, approaching the intrinsic limit of the TDC ASIC, with a single-shot precision equal to 40 ps (FWHM) and an overall DNL equal to 1.2% LSB (RMS). To guarantee real-time acquisitions, compatible with in-vivo measurements, we split the FPGA block Random-Access Memory (RAM) in four sections (two per each time-measurement unit) implementing a memory-swapping algorithm for downloading the reconstructed histogram while another measurement is running, without introducing any dead-time due to data transfer. With this feature, the minimum measurement integration time is equal to 300 ms (only limited by data transfer through the USB), which can be increased up to 16 s per each detection channel, limited by the FPGA RAM size.

III. Experimental Characterization

To assess the performance of the instrument here presented, we carried out its detailed experimental characterization. Results are reported in the following sections.

A. Instrument Response Function

The typical Instrument Response Functions for all the eight wavelengths are shown in Fig. 5. They were acquired directly coupling the 100 μm-core output fiber of the 9×1 optical switch and the 1 mm-core collection fiber, connected to SiPM 2. TDC Unit 2 was used to reconstruct the TCSPC histograms. Each curve was obtained as the sum of 1 s consecutive measurements at 40 MHz repetition rate until the peak count reaches 10^6. The detector count rate was kept always lower than 650 kcps (i.e., $\sim$1.5% of the laser repetition rate) thus keeping the distortion due to pile-up effect well below 1%. As can be seen, by increasing the excitation wavelength (Fig. 5 from panel a to h), the amplitude of the exponential decay increases, as more photons are absorbed within neutral region of the silicon photodetector, thus triggering an avalanche after diffusing towards the depleted region, in agreement with [38].

Measurement results are reported in Table II and IRFs exhibit a temporal duration from 100 to 155 ps (FWHM) depending on the selected wavelength, which, to the best of our knowledge, represent state-of-the-art performance for a complete near-infrared time-resolved spectroscopy system based on pulsed diode lasers and wide-area single-photon detectors.

B. Measurement Stability

Measurement stability over time and temperature is of utmost importance in TD NIRS measurements, as any drift of pulsed laser sources, single-photon detectors or time-measurement units may lead to incorrect estimation of scattering and absorption coefficients, especially when employed outside the controlled environment of the research laboratories. Moreover, a short turn-on time is desirable. In TD-NIRS, DTOF is analyzed considering the IRF in order to estimate accurately absorption and scattering coefficients [7], [8]. As IRF is stable over a long period, it can be acquired just at the beginning of the measurement session, with no need of successive acquisitions.

We tested the instrument measurement stability by acquiring the IRFs of the eight laser sources with 2 s integration time per each wavelength. Within collected data, we identified the first time-interval after turn-on where measurement stability proved

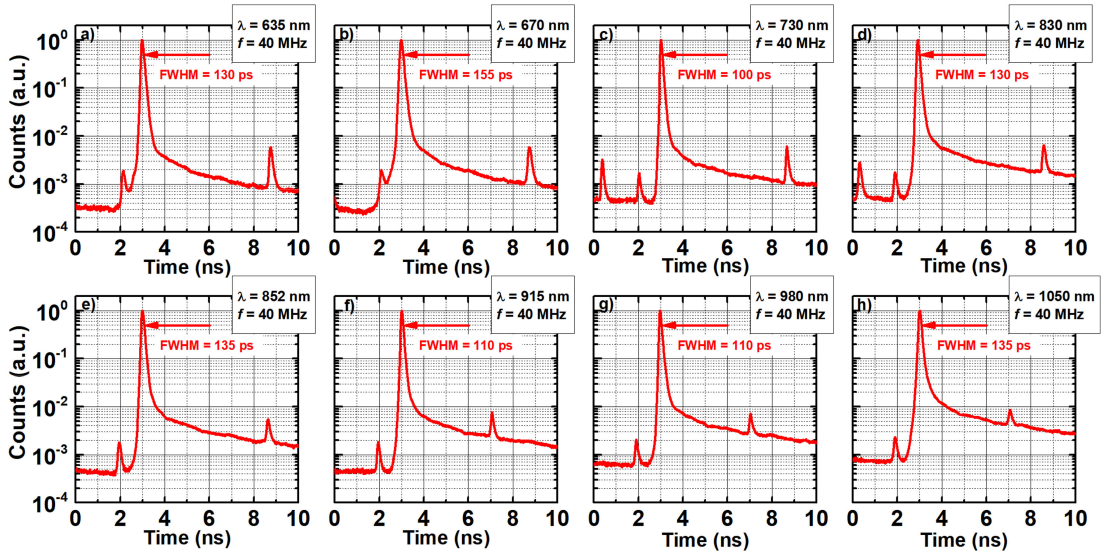

Fig. 5. IRFs of the eight pulsed laser sources. Each IRF curve includes contributions from the laser pulse-width, the SPTR of the single-photon detector (70 ps FWHM) and the single-shot precision of time-measurement unit (40 ps FWHM). Each IRF is normalized to its main peak. Multiple peaks due to signal reflections at fiber junctions are not an issue as the Region-Of-Interest (ROI) of the reconstructed optical pulses for spectroscopic measurement extends exclusively few nanoseconds after the main peak.

TABLE II
OPTICAL PERFORMANCE OF THE DESCRIBED INSTRUMENT

Wavelength [nm]	*IRF* [a] *[ps]*	*Warm-up time* [b] *[min]*
635	130	25
670	155	35
730	100	50
830	130	50
852	135	15
915	115	25
980	110	30
1050	135	15

[a]FullWidth at Half-Maximum.
[b]For 3 hours ±1% measurement stability.

to be better than ±1% for 3 hours. Measurement results proved that optical stability better than ±1% is obtained for all the eight pulsed laser sources and warm-up times are reported in Table II. However, measurement stability requires, besides constant laser output power and detector PDE, negligible drifts of the pulse temporal position (with respect to the measurement synchronization signal) and of the pulse-shape, as any variation of these two parameters may lead to incorrect measurement results. The results of stability measurement for the 852 nm light source are reported in Fig. 6: about 15 minutes after turn-on, the detector count rate is stable within ±1% throughout all the measurement duration (i.e., 6 hours). Moreover, laser pulses exhibit only a few picoseconds temporal shift and the IRF pulse-width is

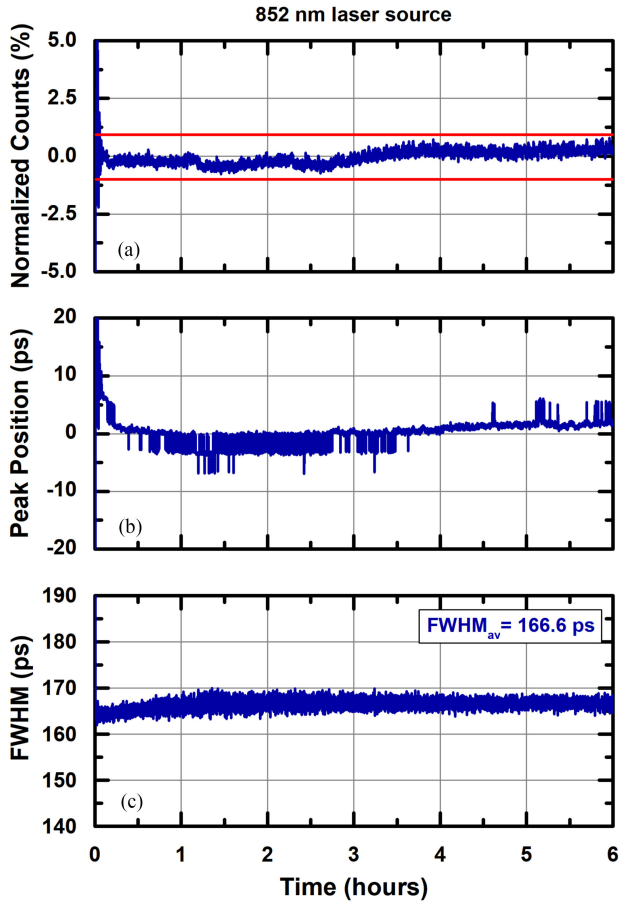

Fig. 6. Measurement stability for the 852 nm pulsed laser source. (a) The counts variation is due to unstable performance of the pulsed laser diode, the single-photon detector (SiPM 2) and the time-measurement unit (TDC Unit 2). The red horizontal lines highlight the ±1% range. (b) Reports the peak position (i.e., the centroid) of the DTOF curves. (c) The pulse-width of the IRF for the selected wavelength.

almost constant. All the pulsed laser sources exhibit comparable stability performance.

C. Differential Non-Linearity

The DNL of the time-measurement unit is given by both non-homogeneity in the temporal bin widths of the TDC ASIC and disturbances coupled to sensitive electrical signals. The latter ones can be strongly reduced with proper design of the timing circuitry, whereas the bin widths cannot be completely corrected with the time-measurement instrument calibration. This may lead to distortion of the reconstructed waveforms, thus altering the results of the spectroscopic measurement.

We tested instrument DNL by acquiring photon counts by one of the two SiPM-based detectors, illuminated by uniform background light, in order to reach a count rate of 400 kcps at 40 MHz repetition rate. The detector output is split into two paths towards both the time-measurement units. In this way, ideally uniform distributions of counts are expected, apart from Poisson noise fluctuations. DTOF curves were integrated for 3 hours to reduce the relative contribution of the Poisson noise, thus improving the definition of the waveform and highlight the DNL pattern. A second acquisition of 100 seconds (100 measurements with 1 s integration time) was performed after some time to verify the possibility to correct the DNL pattern, as reported in [22]. Measurement results are reported in Fig. 7, with both the corrected and uncorrected waveforms for the two detection channels. Summing the TDC histograms of the second acquisition, we obtained an average histogram level of about 15 kcounts on both TDCs, resulting in an expected standard deviation due to Poisson noise of about 122 counts, which normalized with the average count rate results in 0.8% LSB RMS. By computing the standard deviation on the histogram of each TDC, we obtained a fluctuation of about 2% on TDC 1 and of 1.2% on TDC 2, thus suggesting the presence of additional distortion due to the DNL. After correction, both histograms exhibit a residual DNL of 0.8% LSB (RMS).

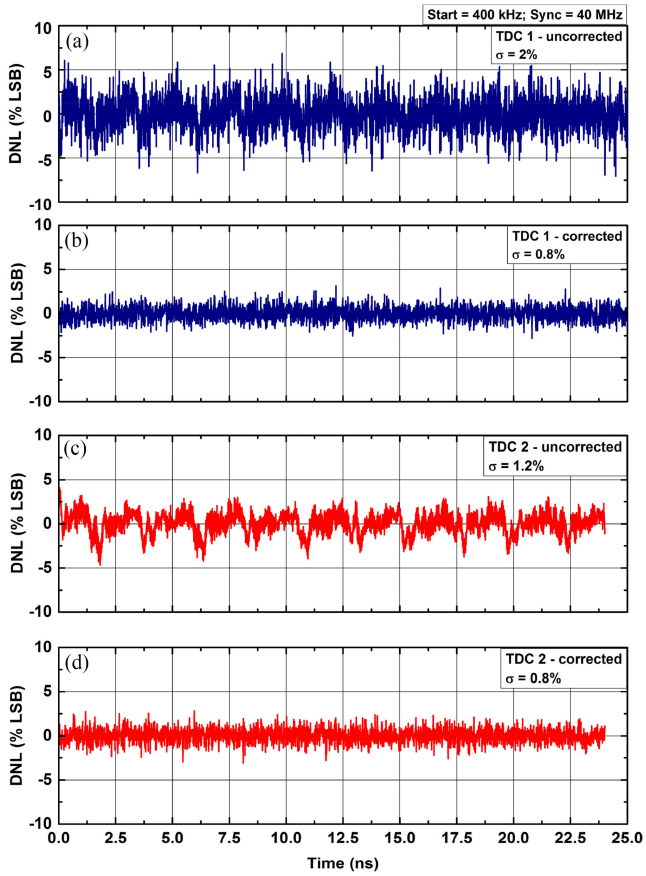

Fig. 7. Distributions of photon time-of-flights under uncorrelated uniform illumination of the SiPM-based detectors, before and after DNL correction for both TDC 1 (a and b – blue lines) and TDC 2 (c and d – red lines). As can be seen, the periodic DNL pattern is effectively suppressed by the post-processing correction algorithm.

D. Validation on Phantoms

Two series of phantoms mimicking optical properties of biological tissues [39] were measured at all the eight wavelengths. In the first series the scattering coefficient is constant (around 10 cm^{-1} at 660 nm) while the absorption coefficient increases linearly (from 0 to 0.49 cm^{-1} by steps of 0.07 cm^{-1} at 660 nm). Phantoms of this series are labelled from 1 to 8. In the second series the absorption coefficient is constant (around 0.07 cm^{-1} at 660 nm) while reduced scattering coefficient increases linearly (from 5 to 20 cm^{-1} by steps of 5 cm^{-1} at 660 nm). Phantoms of this series are labelled from A to D. Measurements were performed at 40 MHz laser pulse repetition rate placing the injection fiber and one of the two detection fibers over the phantom surface with an inter-fiber distance around 2.4 cm. Attenuation was adjusted to obtain a count rate equal to 2 Mcps and 20 repetitions were acquired, with 1 s integration time. To perform the measurement, SiPM 1 and TDC 1 were used.

All the photon DTOF curves acquired were analyzed: after background subtraction, values of absorption and reduced scattering coefficients were extracted with a non-linear optimal fit procedure using an analytical model describing propagation of photons in a homogeneous semi-infinite turbid medium [40]. We report the results in two figures. Fig. 8 shows the linearity of the instrument in estimating absorption (a and b) and reduced scattering (c and d) coefficients. The instrument first four wavelengths are reported in left column (a and c) and the second four wavelengths in right column (b and d). The system shows good linearity in measuring absorption and reduced scattering coefficients, comparable with state-of-the-art diffuse optical spectroscopy systems [41].

In Fig. 9 we show the absorption coefficient spectrum (a) and the reduced scattering coefficient spectrum (b) compared with measurements on the same phantom performed with another state-of-the-art spectroscopy system, which has a discrete number of wavelengths in the near-infrared range (further details about the reference instrument are reported in [42]). The measured phantom has nominal absorption coefficient around 0.07 cm^{-1} at 660 nm and nominal reduced scattering coefficient around 10 cm^{-1} at 660 nm.

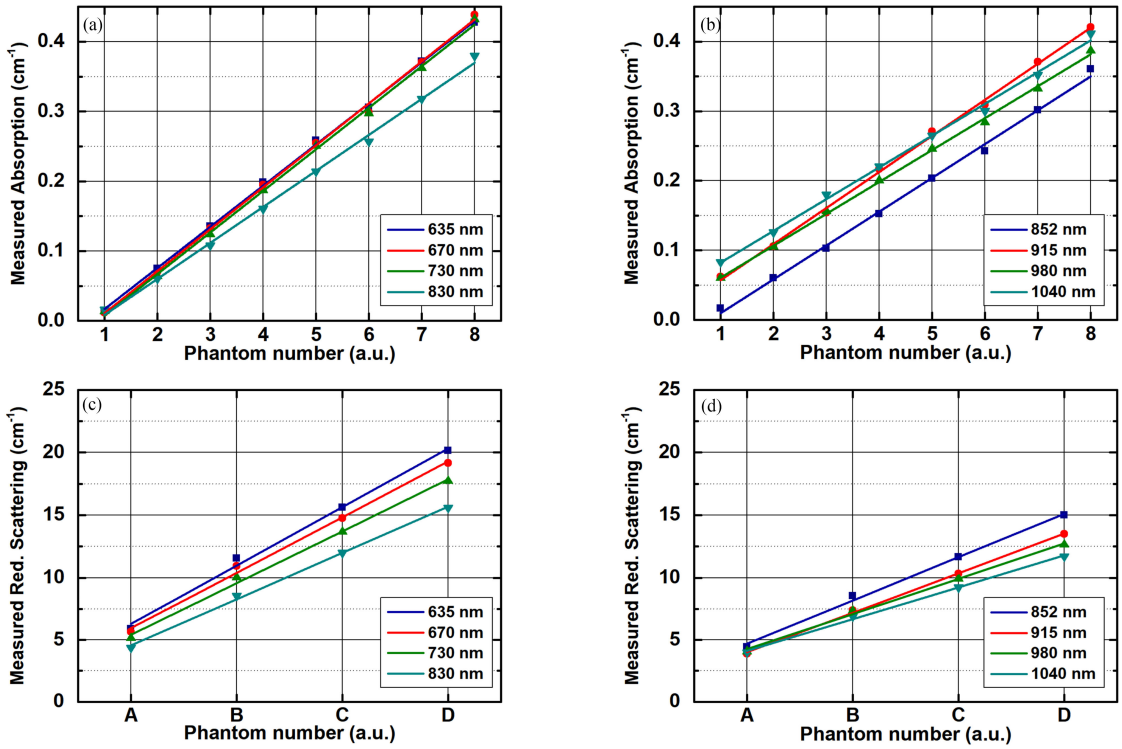

Fig. 8. Linearity on absorption and reduced scattering coefficients. The upper row (a and b) shows the estimated absorption coefficients and the lower row (c and d) shows the estimated reduced scattering coefficients. The results of the first four wavelengths of the instrument are reported in left column (a and c) while the second four wavelengths are reported in right column (b and d). The symbols represent the average results over the 20 repetitions. Error bars are not shown because hidden by the markers on the plots, since the standard deviation over 20 measurements is 2 orders of magnitude lower than the corresponding average value. Phantoms labelled from 1 to 8 have nominal absorption coefficients from 0 to 0.49 cm^{-1} by steps of 0.07 cm^{-1} and nominal reduced scattering coefficient of 10 cm^{-1} at 660 nm, while phantoms labelled from A to D have nominal reduced scattering coefficient from 5 to 20 cm^{-1} by steps of 5 cm^{-1} and nominal absorption coefficient of 0.07 cm^{-1} at 660 nm.

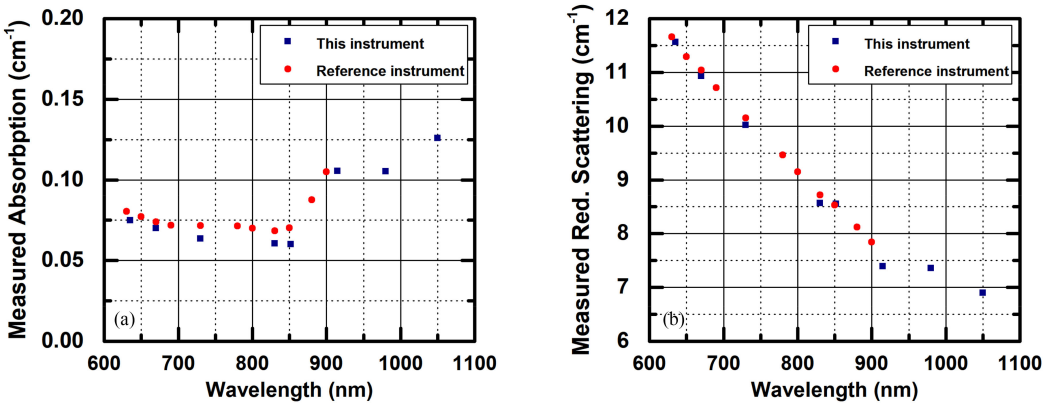

Fig. 9. Comparison of measured absorption and scattering coefficients spectra of the 2B phantom (nominal absorption coefficient of 0.07 cm^{-1} and nominal reduced scattering coefficient of 10 cm^{-1} at 660 nm). Figure a) shows the absorption coefficient spectrum while figure b) the reduced scattering coefficient spectrum, measured with both the presented instrument (squares) and with a state-of-the-art spectroscopy system (dots).

The results presented in Fig. 9 show a good accordance between the two instruments on both absorption and reduced scattering coefficients estimation.

IV. Conclusion

In this paper we presented the design and preliminary characterization of an innovative complete instrument for near-infrared time-resolved spectroscopy featuring eight pulsed diode laser sources emitting at different wavelengths in the near-infrared spectral region, and two detection channels with single-photon detection capability and TCSPC-based time-measurement units. The experimental characterization proved, at all the wavelengths, an average optical power at fiber output higher than 1 mW (at 40 MHz pulse repetition rate), an IRF narrower than 160 ps (FWHM), a DNL equal to 1.2% LSB RMS with 10 ps

timing resolution and stability (better than $\pm 1\%$) over time and ambient temperature for several hours of operation. The high performance of the instrument and the great system reconfigurability (thanks to the all-digital FPGA-based readout electronics) allows to tailor the measurement parameters for a broad range of applications where pulsed laser sources and the TCSPC technique are needed, still guaranteeing real-time data acquisition.

ACKNOWLEDGMENT

This project is an initiative of the Photonics Public Private Partnership (www.photonics21.org).

REFERENCES

[1] J. Johansson *et al.*, "Time-resolved NIR/Vis spectroscopy for analysis of solids: Pharmaceutical tablets," *Appl. Spectrosc.*, vol. 56, pp. 725–731, 2002.
[2] R. Cubeddu *et al.*, "Time-Resolved reflectance spectroscopy applied to the non-destructive monitoring of the internal optical properties in apples," *Appl Spectrosc.*, vol. 55, pp. 1368–1374, 2001.
[3] R. Cubeddu, A. Pifferi, P. Taroni, A. Torricelli, and G. Valentini, "Noninvasive absorption and scattering spectroscopy of bulk diffusive Media: An application to the optical characterization of human breast," *Appl. Phys. Lett.*, vol. 74, pp. 874–876, 1999.
[4] G. Strangman, D. A. Boas, and J. P. Sutton, "Non-invasive neuroimaging using near-infrared light," *Biol. Psychiatry*, vol. 52, pp. 679–693, 2002.
[5] A. P. Gibson and H. Dehghani, "Diffuse optical imaging," *Philosophical Trans. Roy. Soc. A*, vol. 367, no. 1900, pp. 3055–3072, 2009.
[6] T. Durduran, R. Choe, W. B. Baker, and A. G. Yodh, "Diffuse optics for tissue monitoring and tomography," *Rep. Prog. Phys.*, vol. 73, no. 7, Jul. 2010, Art. no. 76701.
[7] A. Ishimaru *Wave Propagation and Scattering in Random Media*. New York, NY, USA: Academic, 1978.
[8] T. Vo-Dhin, *Biomedical Photonics Handbook*. Boca Raton, FL, USA: CRC Press, 2003.
[9] D. Contini *et al.*, "Review: Brain and muscle near infrared spectroscopy/imaging techniques," *J. Near Infrared Spectrosc.*, vol. 20, no. 1, pp. 15–27, 2012.
[10] A. P. Gibson, J. C. Hebden, and S. R. Arridge, "Recent advances in diffuse optical imaging," *Phys. Med. Biol.*, vol. 50, pp. 1–43, 2005.
[11] A. Dalla Mora *et al.*, "Towards next-generation time-domain diffuse optics for extreme depth penetration and sensitivity," *Biomed. Opt. Express*, vol. 6, no. 5, pp. 1749–1760, Apr. 2015.
[12] F. Martelli *et al.*, "There's plenty of light at the bottom: Statistics of photon penetration depth in random media," *Sci. Rep.*, vol. 6, no. 1, Jul. 2016, Art. no. 27057.
[13] S. Del Bianco, F. Martelli, and G. Zaccanti, "Penetration depth of light re-emitted by a diffusive medium: Theoretical and experimental investigation," *Phys. Med. Biol.*, vol. 47, no. 23, pp. 4131–4144, 2002.
[14] J. Steinbrink, H. Wabnitz, H. Obrig, A. Villringer, and H. Rinneberg, "Determining changes in NIR absorption using a layered model of the human head," *Phys. Med. Biol.*, vol. 46, no. 3, pp. 879–896, 2001.
[15] L. Zucchelli, D. Contini, R. Re, A. Torricelli, and L. Spinelli, "Method for the discrimination of superficial and deep absorption variations by time domain fNIRS," *Biomed. Opt. Express*, vol. 4, no. 12, pp. 2893–2910, 2013.
[16] A. Puszka *et al.*, "Spatial resolution in depth for time-resolved diffuse optical tomography using short source-detector separations," *Biomed. Opt. Express*, vol. 6, no. 1, pp. 1–10, Jan. 2015.
[17] A. Pifferi *et al.*, "Time-resolved diffuse reflectance using small source-detector separation and fast single-photon gating," *Phys. Rev. Lett.*, vol. 100, no. 13, 2008, Art. no. 138101.
[18] E. Alerstam *et al.*, "Single-fiber diffuse optical time-of-flight spectroscopy," *Opt. Lett.*, vol. 37, no. 14, pp. 2877–2879, Jul. 2012.
[19] A. Pifferi *et al.*, "New frontiers in time-domain diffuse optics, a review," *J. Biomed. Opt.*, vol. 21, no. 9, Jun. 2016, Art. no. 091310.
[20] L. Di Sieno *et al.*, "Miniaturized pulsed laser source for time-domain diffuse optics routes to wearable devices," *J. Biomed. Opt.*, vol. 22, no. 8, Aug. 2017, Art. no. 085004.
[21] J. Bouchard *et al.*, "A low-cost time-correlated single photon counting system for multiview time-domain diffuse optical tomography," *IEEE Trans. Instrum. Meas.*, vol. 66, no. 10, pp. 2505–2515, Oct. 2017.
[22] M. Buttafava *et al.*, "A compact two-wavelength time-domain NIRS system based on SiPM and pulsed diode lasers," *IEEE Photon. J.*, vol. 9, no. 1, Feb. 2017, Art. no. 7800114.
[23] B. Markovic, S. Tisa, F. A. Villa, A. Tosi, and F. Zappa, "A high-linearity, 17 ps precision time-to-digital converter based on a single-stage Vernier delay loop fine interpolation," *IEEE Trans. Circuits Syst. I, Reg. Papers*, vol. 60, no. 3, pp. 557–569, Mar. 2013.
[24] A. Pifferi *et al.*, "Fully automated time domain spectrometer for the absorption and scattering characterization of diffusive media," *Rev. Sci. Instrum.*, vol. 78, no. 5, 2007, Art. no. 053103.
[25] NKT Photonics, "SuperK supercontinuum sources," [Online]. Available: https://www.nktphotonics.com/lasers-fibers/product-category/supercontinuum-lasers. Accessed on: Mar. 10, 2018.
[26] Becker and Hickl Gmbh, "BDS-MM family picosecond diode lasers," [Online]. Available:http://www.becker-hickl.de/pdf/db-bds-mm-family-08.pdf. Accessed on: Mar. 3, 2018.
[27] P. Gmbh, "LDH Series – Picosecond pulsed diode laser heads," [Online]. Available: https://www.picoquant.com/products/category/picosecond-pulsed-sources/ldh-series-picosecond-pulsed-diode-laser-heads. Accessed on: Mar. 3, 2018.
[28] P. Paulus, R. Langenhorst and D. Jager, "Generation and optimum control of picosecond optical pulses from gain-switched semiconductor lasers," *IEEE J. Quantum Electron.*, vol. 24, no. 8, pp. 1519–1523, Aug. 1988.
[29] K. K. Hamamatsu Photonics, "*Photomultiplier Tube Handbook*, 2007.
[30] A. Gulinatti, P. Maccagnani, I. Rech, M. Ghioni, S. Cova, "35 ps time resolution at room temperature with large area single photon avalanche diodes," *IET Electron. Lett.*, vol. 41, no. 5, pp. 272–274, Mar. 2005.
[31] M. Sanzaro *et al.*, "Single-photon avalanche diodes in a 0.16 μm BCD technology with sharp timing response and red-enhanced sensitivity," *IEEE J. Sel. Topics Quantum Electron.*, vol. 24, no. 2, Mar./Apr. 2018, Art. no. 3801209.
[32] A. Dalla Mora *et al.*, "Fast silicon photomultiplier improves signal harvesting and reduces complexity in time-domain diffuse optics," *Opt. Express*, vol. 23, no. 11, pp. 13937–13946, May 2015.
[33] E. Martinenghi *et al.*, "Spectrally resolved single-photon timing of silicon photomultipliers for time-domain diffuse optics," *IEEE Photon. J.*, vol. 7, no. 4, Aug. 2015, Art. no. 6802512.
[34] E. Martinenghi *et al.*, "Time-resolved single-photon detection module based on silicon photomultiplier: A novel building block for time-correlated measurement systems," *Rev. Sci. Instrum.*, vol. 87, 2016, Art. no. 073101.
[35] P. Gmbh, "HydraHarp 400-multichannel picosecond event timer & TCSPC module," [Online]. Available: https://www.picoquant.com/products/category/tcspc-and-time-tagging-modules/hydraharp-400-multichannel-picosecond-event-timer-tcspc-module. Accessed on: Mar. 10, 2018.
[36] Becker and H.ickl Gmbh, "SPC-130 low cost TCSPC module," [Online]. Available: http://www.becker-hickl.de/pdf/dbspc130-2.pdf. Accessed on: Mar. 10, 2018.
[37] M. Renna *et al.*, "Compact dual-wavelength system for time-resolved diffuse optical spectroscopy," in *Proc. 13th Conf. Ph.D. Res. Microelectronics Electron.*, Giardini Naxos, 2017, pp. 293–296.
[38] E. Martinenghi *et al.*, "Spectrally resolved single-photon timing of silicon photomultipliers for time-domain diffuse spectroscopy," *IEEE Photon. J.*, vol. 7, no. 4, Aug. 2015, Art. no. 6802512.
[39] A. Pifferi "Performance assessment of photon migration instruments: The MEDPHOT protocol," *Appl. Opt.*, vol. 44, no. 11, pp. 2104–2114, 2005.
[40] F. Martelli, S. Del Bianco, A. Ismaelli, and G. Zaccanti, *Light Propagation through Biological Tissue*. SPIE, 2010.
[41] S. Konugolu Venkata Sekar *et al.*, "Broadband (600–1350 nm) time-resolved diffuse optical spectrometer for clinical use," *IEEE J. Sel. Topics Quantum Electron.*, vol. 22, no. 3, May/Jun. 2016, Art. no. 7100609.
[42] P. E. Zerbini *et al.*, "Optical properties, ethylene production and softening in mango fruit," *Postharvest Biol. Technol.*, vol. 101, pp. 58–65, 2015.

Marco Renna was born in Italy in 1991. He received the M.Sc. degree in electronics engineering from Politecnico di Milano, Milan, Italy, in September 2016. He is currently working toward the Ph.D. degree in information technology with the Dipartimento di Elettronica, Informazione e Bioingegneria, Politecnico di Milano, Milano, Italy. His research interests focuses on the design and development of pulsed laser sources based on laser diodes and time-correlated single-photon counting electronics.

Mauro Buttafava received the Graduate degree in electronics engineering in 2013 and in 2017 and the Ph.D. degree (*cum laude*) in information technology, both from Politecnico di Milano, Milano, Italy. He is currently a Postdoctoral Researcher with the Department of Electronics, Information and Bioengineering, Politecnico di Milano. His research interests include design and characterization of time resolved, gated-mode single photon counting systems. His expertise covers different applications in research, industrial and biomedical fields (like optical spectroscopy, ultrafast time-of-flight imaging and fluorescence microscopy systems design).

Anurag Behera was born in India in 1994. He received the Master's degree in physics with a specialization in photonics from Sri Sathya Sai Institute of Higher Learning, Prasanthi Nilayam, India, in 2016 and is currently working the Ph.D. in physics from the Politecnico di Milano, Milan, Italy, in the field of biomedical optics. His current research interests include the development of devices and methodologies for brain imaging.

Marta Zanoletti was born in Lodi in 1991. She received the Master's degree in physics engineering from the Politecnico di Milano, Milano, Italy, in December 2015 with the experimental thesis: "Dispositivo medico per il monitoraggio dell'ossigenazione cerebrale mediante spettroscopia nel vicino infrarosso risolta in tempo." From May 2016, she is working toward the Ph.D. degree with the Department of Physics, Politecnico di Milano.

Laura Di Sieno received the Master's degree in electronics engineering from the Politecnico di Milano, Milano, Italy, in 2011 and the Ph.D. degree in physics from the same university in 2015. Since January 2015, she has been a Postdoctoral Fellow. Her research interests include study and application of instrumentation for time-resolved optical spectroscopy of highly scattering media using single-photon detectors.

Alberto Dalla Mora received the Master's degree (*cum laude*) in electronics engineering and the Ph.D. degree in information and communication technology from the Politecnico di Milano, Milano, Italy, in 2006 and 2010, respectively. He is currently an Associate Professor of physics with Politecnico di Milano, Italy. He authored about 50 papers in international peer-reviewed journals and more than 45 conference proceedings. His research interests include time-resolved diffuse optics techniques and instrumentation for biomedical applications.

Davide Contini was born in Angera, Italy, in 1978. He received the Master's degree in electronic engineering and the Ph.D. degree in physics from the Politecnico di Milano, Milano, Italy, in 2003 and 2007, respectively. Since 2014, he has been an Associate Professor of physics with the Politecnico di Milano. His current research interests include the interaction of laser light with matter, and in particular the time-resolved spectroscopy of highly diffusive media for applications in biology and medicine.

Alberto Tosi (M'07) was born in Borgomanero, Italy, in 1975. He received the Master's degree in electronics engineering and the Ph.D. degree in information technology engineering from the Politecnico di Milano, Milano, Italy, in 2001 and 2005, respectively. He was an Assistant Professor from 2006 to 2014. He has been an Associate Professor of electronics with the Politecnico di Milano since 2014. In 2004, he was a Student with the IBM T. J. Watson Research Center, Yorktown Heights, NY, working on optical testing of CMOS circuits. He is currently working on silicon and InGaAs/InP single-photon avalanche diodes. His research interests include arrays of silicon SPADs for 2-D and 3-D applications and time-correlated single-photon counting electronics.